30 Mar 2001, 10:30 am - 12:30 pm

Numerical Analysis for Seismic Behavior of a Slope Based on a Simple Cyclic Loading Model

Akihiko Wakai
Gunma University, Japan

Keizo Ugai
Gunma University, Japan

Masayoshi Sato
Japan National Research Institute for Earth Science and Disaster Prevention, Japan

Takashi Tazo
Shimizu Co., Ltd., Japan

NUMERICAL ANALYSIS FOR SEISMIC BEHAVIOR OF A SLOPE BASED ON A SIMPLE CYCLIC LOADING MODEL

Akihiko Wakai & Keizo Ugai
Department of Civil Engineering
Gunma University
Kiryu, Gunma 376-8515, JAPAN

Masayoshi Sato
Japan National Research Institute
for Earth Science and Disaster Prevention
Tsukuba, Ibaraki 305-0006, JAPAN

Takashi Tazo
Institute of Technology
Shimizu Co., Ltd.
Tokyo 135-8530, JAPAN

ABSTRACT

A finite element simulation for dynamic centrifuge test of a slope is presented. The horizontal acceleration was applied to the base of the ground, and the response of the slope was measured. The residual deformation, accompanied with a clear slip surface, was observed after the testing. The main objective of this study is to investigate the validity of a new cyclic loading model, based on the strength parameters c-ϕ, and the $G-\gamma$, $h-\gamma$ relationships. These features are thought to be very useful for practical usage.

INTRODUCTION

Solutions derived from a seismic stability analysis for slopes, based on the limit equilibrium method, are sometimes very conservative, because the seismic force is assumed to be acting constantly and the amplification of response is not taken into account in such methods. On the other hand, it has been confirmed that the numerical analysis such as the dynamic elasto-plastic finite element method (FEM) is very effective for the evaluation of the seismic stability of slopes. There have been many inspiring papers about the dynamic elasto-plastic FE analyses for slopes without typical liquefiable layers, e.g., Toki et al. (1985), Griffiths et al. (1988), Woodward et al. (1994), Ugai et al. (1996), Iai et al. (1999) and Uzuoka (2000).

Background of the Proposed Model

Wakai et al. (1999) has reported finite element simulations for a dynamic centrifuge model test of an embankment on the soft clayey ground. In the experiment, the ground under the embankment was largely deformed after earthquake. Those results could be simulated well by the 2D dynamic elasto-plastic FEM. They have concluded that the hysteretic characteristics such as the $G-\gamma$, $h-\gamma$ relationships are very important to analyze those problems. In their analyses, a newly proposed cyclic loading model was applied to the soft clayey ground. This constitutive model is based on the shear modulus G_0, and the undrained shear strength c_u for $\phi = 0$ materials. An advantage of their constitutive model is that the $G-\gamma$ and $h-\gamma$ relationships of soils are properly taken into account. Besides, the number of parameters needed for the analyses is very low, and this feature is very useful for practical usage. On the other hand, a defect of this model was that the strength parameters c and ϕ in Mohr-Coulomb's criterion, often used in the stability problems for geotechnical structures, cannot be adopted.

A Simple Cyclic Loading Model

The model presented in this paper is a modification of the previous Ugai-Wakai's constitutive model (Wakai et al., 1999) for $\phi = 0$ materials. The main objective of this study is to investigate the validity of a new cyclic loading model, based on the shear strength c-ϕ, and the $G-\gamma$, $h-\gamma$ relationships.

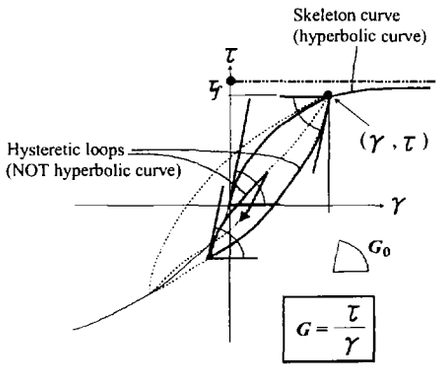

Fig. 1. Hysteretic curves in stress-strain relationship.

A SIMPLE CYCLIC LOADING MODEL FOR $c-\phi$ MATERIALS

Basic Assumptions

Before describing the details of the new cyclic loading model, we should discuss the basic assumptions in its formulations.

(a) Liquefaction and any other cyclic softening or hardening behaviors do not occur during loading.
(b) Cyclic behaviors can be represented by the shear stress τ – shear strain γ relationships.
(c) The initial inclination of both the skeleton curve and the hysteretic loops are consisitent ($=G_0$).
(d) Masing's rule is not adopted.

Although some parts of these assumptions seem to have weaker theoretical background, they are very useful in simplifying the formulations.

Skeleton Curve

In this model, the skeleton curve is assumed to be a hyperbolic curve (Fig.1), given by

$$\bar{\tau} = \frac{G_0 \bar{\gamma}}{1 + \dfrac{G_0 \bar{\gamma}}{\tau_f}} \tag{1}$$

where

$$\bar{\tau} = \tau(\{\sigma\} - \{\sigma_0\}) \tag{2a}$$
$$\bar{\gamma} = \gamma(\{\varepsilon\} - \{\varepsilon_0\}) \tag{2b}$$

The symbols with "0" denote the initial values. Eq.(1) has two parameters G_0 and τ_f. The value of G_0 is assumed to be constant in this study, although it is possible to be varied, according to the change of the mean principal stress. Young's modulus E is given by $2G_0(1+\nu)$. ν is Poisson's ratio. The form of skeleton curve is similar to the Hardin-Drnevich model (Hardin et al., 1972). The deviatoric stress and strain invariants are given by

$$\tau(\{\sigma\}) = \tau_{max} = \sqrt{J_2}\sin\left(\frac{\pi}{3} + \Theta\right) \tag{3a}$$
$$\gamma(\{\varepsilon\}) = \gamma_{max} = 2\sqrt{J_2^*}\sin\left(\frac{\pi}{3} + \Theta^*\right) \tag{3b}$$

Θ and Θ^* are Lode angles in the stress and strain space, respectively. The shear strength τ_f is given by

$$\tau_f = c\cdot\cos\phi + \frac{\sigma_1 + \sigma_3}{2}\sin\phi \tag{4}$$

c and ϕ are the strength parameters in Mohr-Coulomb's failure criterion. The flow rule is derived from Rowe's stress-dilatancy relationships. Therefore, the plastic potential g in plane strain condition (Manassero, 1989) is given by

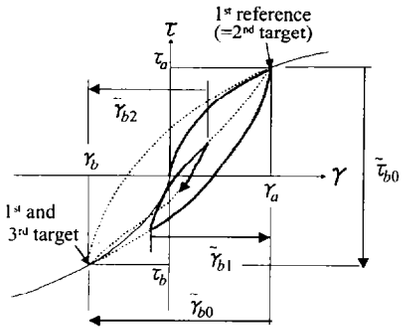

Fig. 2. Concept of stress reversal and reference points.

$$g = \frac{\sigma_1^{K_{cv}}}{\sigma_3} \tag{5}$$

K_{cv} is a constant which corresponds to the stress ratio at the phase transformation. Therefore, when $\sigma_1/\sigma_3 > K_{cv}$, the soil swells; $\sigma_1/\sigma_3 < K_{cv}$, the soil contracts. If $\sigma_3 \le 0$, Eq.(5) is replaced by the plastic potential function based on von Mises equation $g = \sqrt{J_2}$.

Hysteretic Loops

Masing's rule is not adopted and the hysteretic loop are given by

$$\tilde{\tau} = \frac{a\tilde{\gamma}^n + G_0\tilde{\gamma}}{1 + b\tilde{\gamma}} \tag{6}$$

where the local values of τ and γ are defined as

$$\tilde{\tau} = \tau(\{\sigma\} - \{\sigma_a\}) \tag{7a}$$
$$\tilde{\gamma} = \gamma(\{\varepsilon\} - \{\varepsilon_a\}) \tag{7b}$$

$(\gamma_a, \tau_a) = (\gamma(\{\varepsilon_a\}), \tau(\{\sigma_a\}))$ is the reference stress point which corresponds to the newest reversal point in the stress-strain history as shown in Fig. 2. Unloading occurs when the shear strain increment $d\gamma < 0$ is satisfied. If the next target point, which is the terminal point of the current hysteretic loop including the present stress point, is represented as $(\gamma_b, \tau_b) = (\gamma(\{\varepsilon_b\}), \tau(\{\sigma_b\}))$, the value of a is given by

$$a = \frac{1}{\tilde{\gamma}_b^n}\{\tilde{\tau}_b(1 + b\tilde{\gamma}_b) - G_0\tilde{\gamma}_b\} \tag{8}$$

Eq.(8) provides the condition of geometrical compatibility so that the current hysteretic loop should pass through the next target point (γ_b, τ_b).

After the stress path reaches the target point, it has to be recovered on the skeleton curve. On the other hand, if the stress

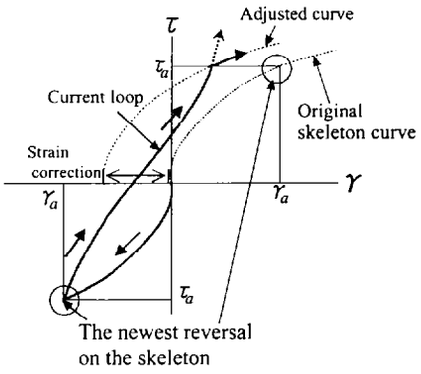

Fig. 3. Adjustment of the skeleton curve.

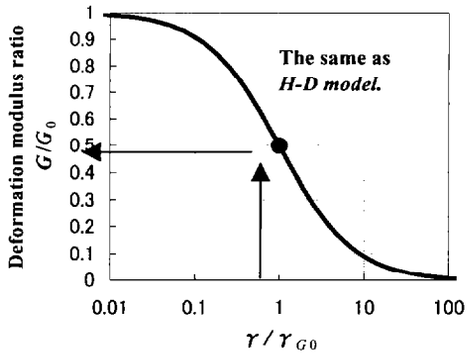

Fig. 4. Assumed $G-\gamma$ relationship in the proposed model.

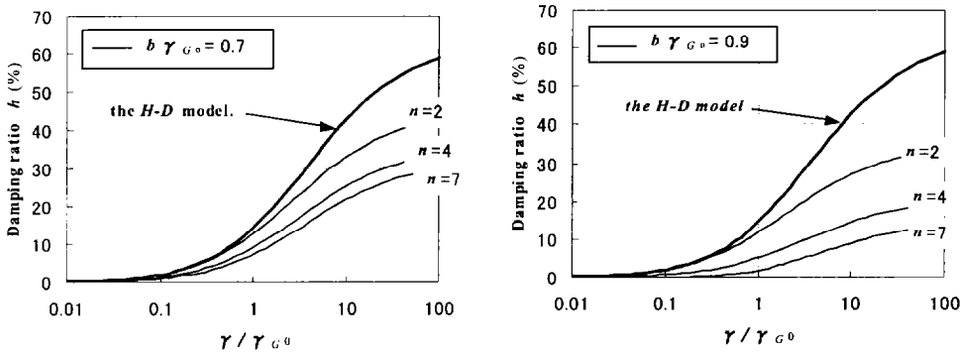

Fig. 5. $h-\gamma$ relationships in cases where $b\gamma_{G_0}$ = 0.7 and 0.9 are given.

path is reversed (i.e., $d\tilde{\gamma} < 0$ is satisfied) halfway on a hysteretic loop, the present point becomes a new reference point according to local values $\tilde{\tau}$ and $\tilde{\gamma}$. Also, the new values of $\tilde{\tau}_b$ and $\tilde{\gamma}_b$ are given by the distance from the stress point (γ_a, τ_a) which is the next target point of the current hysteretic loop. Of course, the value of a should be changed. After that, if the stress path is again reversed halfway, the present point becomes a new reference point again, and the new values of $\tilde{\tau}_b$ and $\tilde{\gamma}_b$ are given by the distance from the target point (γ_b, τ_b) as shown in Fig. 2. However, it sometimes happens that before the stress path reaches the target point on a hysteretic loop, the value of $\tilde{\tau}$ becomes greater than the maximum of τ in history. In this case, the shape of the skeleton curve has to be adjusted so that the current hysteretic loop is smoothly changed to the skeleton curve, as shown in Fig. 3.

$G-\gamma$ and $h-\gamma$ Relationships

G_0, τ_f, b and n are determined so that the analytical $G-\gamma$ and $h-\gamma$ relationships should be fitted to the actual hysteretic characteristics of soils. G_0 and τ_f decide the $G-\gamma$ curve as shown in Fig. 4. G $(=\tau/\gamma)$ is the equivalent shear modulus. In this figure, the strain amplitude γ is normalized based on the reference strain γ_{G_0} $(=\tau_f/G_0)$ which corresponds to $G = 0.5 \cdot G_0$. This is the same property as in the H-D model. b and n decide the $h-\gamma$ curve as shown in Fig. 5. In the graphs, the parameter b is expressed as $b \cdot \gamma_{G_0}$ which is the product of b and γ_{G_0}. The area of the enclosed hysteretic loops is calculated by numerical integrations to give these $h-\gamma$ relationships. It can be seen that the increase of b and n, decreases the magnitude of the damping ratio h. In general use, $b \cdot \gamma_{G_0} \geq 0.5$ and $n > 1$ are recommended. It is found that in cases where $b \cdot \gamma_{G_0}$ equals 0.5, $h-\gamma$ curve corresponds to the one derived from the H-D model with Masing's rule. As seen in the figure, if such a relationship is adopted, h is overestimated in the region of large strain. This curve is far removed from the actual property of soils.

Verification for the Stress-Dilatancy Characteristics of the Proposed Model

In order to verify the analytical model proposed in this paper, taking note of its stress-dilatancy relationship during cyclic loading, we have tried to perform numerical simulations for drained cyclic torsional shear tests performed by Pradhan et al. (1989). Fig. 6 shows the experimental results and their nu-

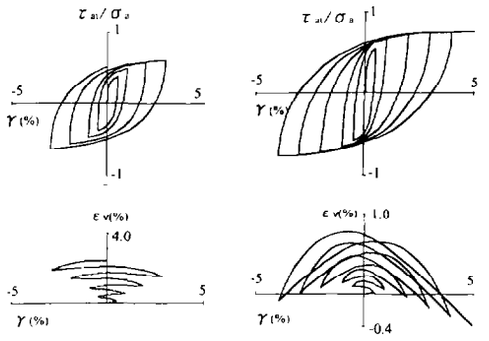

(a) loose sand (b) dense sand

Experiment; Pradhan et al. (1989)

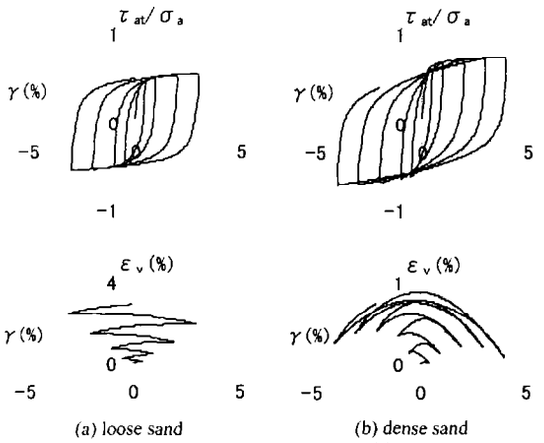

(a) loose sand (b) dense sand

Analytical model proposed in this paper

Fig. 6. Simulations for drained cyclic torsional tests of sand.

Table. 1. Material constants used in the simulation of sand.

	E (kPa)	ν	c (kPa)	ϕ (deg)	K_{cv}	$b \cdot \gamma_{G0}$	n
Loose	150000	0.30	0	35.	3.5	0.60	1.2
Dense	180000	0.30	0	50.	3.5	0.80	1.5

merical simulations based on the model proposed in this paper. The material constants used in the analyses are shown in Table 1. In two tests for loose and dense Toyoura sand, the amplitude of shear distortion was increased with cyclic loading as shown in the figure. In the case for dense sand, the phase transformation can be seen during each cyclic loading, while in the case for loose sand, the volume of the specimen constantly keeps on decreasing. The results of the tests and the analyses agree well with each other.

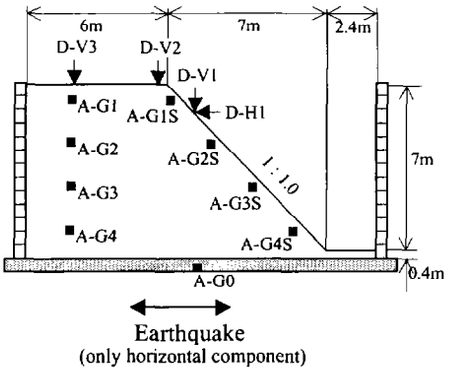

Fig. 7. Dynamic centrifuge test for a model simple slope.

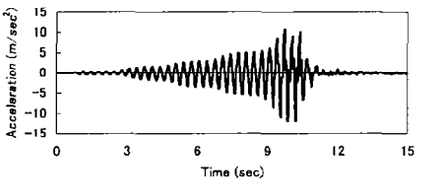

Fig. 8. Input horizontal acceleration in the centrifuge test.

CENTRIFUGE TEST AND ITS NUMERICAL SIMULATION BASED ON DYNAMIC FINITE ELEMENT METHOD

Centrifuge Test of a Model Simple Slope

Dynamic centrifuge model test is very useful for obtaining data to investigate the seismic behavior of geotechnical structures, e.g., slopes, walls and foundations. In this study, we have performed the shaking table test of a slope under centrifugal acceleration. In the experiment, the slope is made of homogenious and unsaturated silty clay (DL clay). The relative density of the soil is about 75%. The centrifugal acceleration of the test is 20G. Fig. 7 shows the sketch of a model slope in the prototype scale, that is, 20 times as the size of the real model. As seen in the figure, the height and the inclination of the slope are 7.0m and 45°, respectively. The points where the history of response is measured are plotted in the figure. The symbols of "D" and "A" denote the measurement of displacement and acceleration, respectively. The point of A-G0 on the shaking table is prepared for the measurement of the base acceleration, i.e., the input horizontal waves. The history of the input waves is shown in Fig. 8. After the testing, we observed the residual deformation accompanied with a slip surface induced during earthquake.

Analytical Model for the Simulation of Centrifuge Test

Fig. 9 shows the sketch of 2D FE meshes in the prototype scale. In the analysis, the bottom of the ground is perfectly fixed and

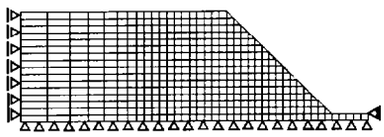

Fig. 9. Finite element meshes used in the simulation.

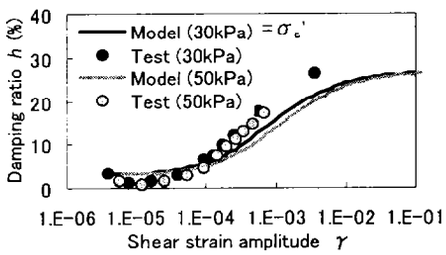

Fig. 10. Assumed $h-\gamma$ relationships in the model.

Table. 2. Material constants used in the simulation of centrifuge test.

E (kPa)	ν	c (kPa)	ϕ (deg)	K_{cv}	$b\cdot\gamma_{G0}$	n	γ_t (kN/m^3)
17000	0.40	11.1	33.3	3.24	8.0	1.5	15.7

be moved vertically. The finite element used in the analysis is 8-nodes iso-parametric element with 4-points reduced integration. Table 2 shows the material constants used in the analysis. Most of these have been determined by the results of drained triaxial compression tests. The strength parameters c and ϕ were evaluated based on the geometry of the Mohr-Coulomb's failure line for the peak strength, in the cases where the confining pressure σ_c'= 19.6, 49, 98, 196kPa. E was assumed to be equal to $2\times E_{50}$, according to the geometrical relationship for a hyperbolic curve. E_{50} is the secant elastic modulus, and was evaluated by the stress-strain curve obtained from a series of triaxial compression tests. In this case, the value of E_{50} was found to be almost constant in the region such that σ_c'= 19.6 to 98 kPa. Shear modulus G_0 was calculated by $0.5E/(1+\nu)$. ν was assumed to be 0.40. The value of K_{cv} was evaluated by the inclination of the regression line for the collection of $(\sigma_1/\sigma_3,\ -2d\varepsilon_3/d\varepsilon_1)$ plot, obtained from the stress-strain curves.

The assumed $h-\gamma$ curves based on the analytical model with parameters in Table 2, when the confining pressure σ_c'=30, 50kPa, are compared with the experimental curves obtained by undrained cyclic triaxial compression tests, as shown in Fig. 10. Here, it should be noted that $h\approx 3\%$ Rayleigh damping is also introduced in the analysis. Therefore, the analytical values of h plotted in the figure are the summation of (i) the hysteretic damping induced by plasticity and (ii) the viscous damping based on Rayleigh damping, 3%. It is found that these $h-\gamma$ curves agree well each other.

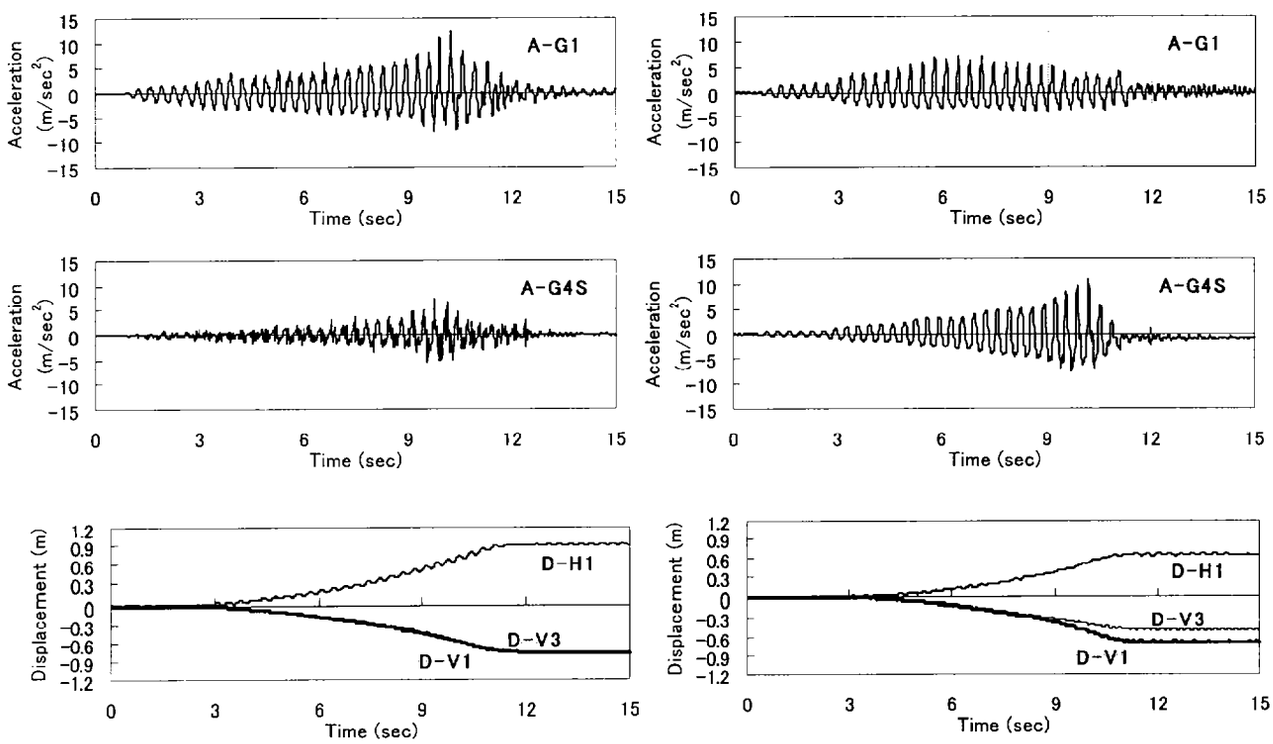

(a) Analytical Results obtained by FEM (b) Experimental Results

Fig. 11. Time histories of acceleration and displacement at each point in the slope.

Comparison of Results; Histories of Acceleration and Displacement

Fig. 11 shows the time histories of horizontal acceleration at each point (A-G1, A-G4S), vertical and horizontal displacement at each point (D-H1, D-V1, D-V3). Both the calculated and the measured results are presented in the figures. A good agreement between FEM and the centrifuge test can be seen in these figures. It is found that the waves of A-G1 and A-G4S are deflected to positive side, i.e., the opposite direction of sliding. In the experiment, it is found that the amplitude of the acceleration response at A-G1 gradually increases in the first half of the history, while it reaches its ceiling in the latter half. This may be caused by the strain-softening behavior of soil during cyclic loading, and the appearance of a few slight cracks on the top. The final values of vertical displacement at D-V1 and D-V3 are almost the same in the analysis, although they are a little different each other in the experiment. In order to simulate such experimental results precisely, it is desirable that the existence of a discontinuous deformation along the slip surface is taken into account in the analysis. The calculated residual deformation of the slope after earthquake is shown in Fig. 12. The slip surface, which is recognized as the area of higher shear strain, is clearly observed in the slope. Large settlement and small upheaving can be seen at the top and the toe of the slope, respectively. These features are almost similar to the experimental result shown in Fig. 13.

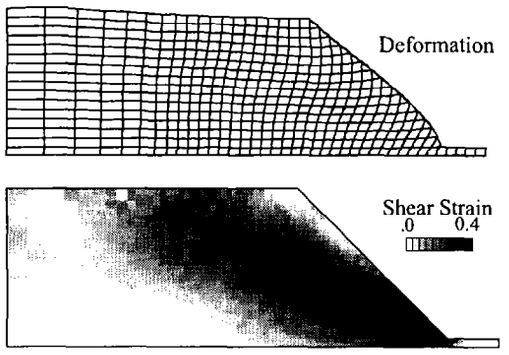

Fig. 12. Residual deformation after earthquake (FEM).

Fig. 13. Residual deformation after earthquake (centrifuge).

CONCLUSIONS

The results observed in the centrifuge test for a model slope are simulated well by the 2D dynamic elasto-plastic FEM. A newly proposed cyclic loading model is found to be very effective for the actual seismic design of slopes, because the number of parameters used in the model is very low.

REFERENCES

Griffiths, D.V. and Prevost, J.N. [1988] Two- and three-dimensional dynamic finite element analyses of the Long Valley Dam@, Geotechnique, Vol.38, No.3, pp.367-388.

Hardin, B.O. and Drnevich, V.P. [1972] Shear modulus and damping in soils : Design equations and curves@, Proc.ASCE, No.SM7, Vol.98, pp.667-692.

Iai, S., Ichii, K., Sato, Y. and Kuwazima, R. [1999] Earthquake response analysis of a high embankment on an existing hill slope @, 2nd International Conference on Earthquake Geotechnical Engineering, pp.697-702, Lisboa, Portugal.

Manassero, M. [1989] Stress-strain relationship from drained self-boring pressuremeter tests in sands@, Geotechnique, Vol.39, No.2, pp.293-307.

Pradhan, T.B.S., Tatsuoka, F. and Sato, Y. [1989] Experimental stress-dilatancy relations of sand subjected to cyclic loading@, Soils and Foundations, Vol.29, No.1, pp.45-64.

Toki, K., Miura, F. and Oguni, Y. [1985] Dynamic slope stability analyses with a non-linear finite element method@, Earthquake Engineering and Structural Dynamics, Vol.13, pp.151-171.

Ugai, K., Wakai, A. and Ida, H. [1996] Static and dynamic analyses of slopes by the 3-D elasto-plastic FEM@, Proc. of 7th International Symposium on Landslides, pp.1413-1416, Trondheim, Norway.

Uzuoka, R. [2000] Analytical study on the mechanical behavior and prediction of soil liquefaction and flow@, A doctoral dissertation of Gifu University, Japan (in Japanese), pp.161-170.

Wakai, A. and Ugai, K. [1999] Evaluation of residual displacement of slopes during earthquake based on a simple cyclic loading model@, 2nd International Conference on Earthquake Geotechnical Engineering, pp.685-690, Lisboa, Portugal.

Woodward, P.K. and Griffiths, D.V. [1994] Non-linear dynamic analysis of the Long Valley Dam@, Computer Methods and Advances in Geomechanics, Balkema, pp.1005-1010.